FMS Images from carbonates of the Bahama Bank Slope, ODP Leg 166: Lithological identification and cyclo-stratigraphy

TREVOR WILLIAMS[1] & CARLOS PIRMEZ[2,3]

[1] *Department of Geology, University of Leicester, Leicester, LE1 7RH, UK (e-mail: tw7@le.ac.uk)*

[2] *Borehole Research Group, Lamont Doherty Earth Observatory, Palisades, NY, USA*

[3] *Now at: Exxon Production Research Co., PO Box 2189, Houston, TX 77252, USA*

Abstract: Ocean Drilling Program (ODP) Leg 166 cored a transect of holes through the prograding carbonate sequences that form the western slope of the Great Bahama Bank, with the aim of detailing the relationship between the sequences and changes in sea-level over the last 25 Ma. A total of 1200 m of FMS resistivity images from Site 1003 (lower slope) and Site 1005 (mid-slope) were divided into three image facies types, with the aid of calibration against the recovered core. Type 1 was conductive (poorly cemented) sediment dominated by pelagic components, Type 2 was resistive (well cemented) sediment dominated by platform (neritic) components, and Type 3 was highly resistive (very well cemented) sediment, usually calci-turbidites but occasionally hardgrounds. Much of the section is composed of metre-scale alternations between Type 1 and Type 2 sediment. We have used the cycle thicknesses in the Middle Miocene to obtain a sedimentation rate curve and to refine the biostratigraphy. The cyclicity is modulated by the precessional astronomical cycle. The FMS images were used to evaluate the lithostratigraphic position and significance of prominent isolated uranium peaks. The peaks tend to occur just below the tops of calci-turbidite-rich units, sometimes coincident with sequence boundaries and maximum flooding surfaces.

Leg 166 of the Ocean Drilling Program sailed from February to April 1996, and drilled a total of seven sites, including a transect of four deep sites, on the western slope of the Great Bahama Bank (Figs 1, 2) (Eberli *et al*. 1997, Anselmetti *et al*. in press). The four deep sites were logged, providing nearly 2 km of FMS images and over 3 km of conventional logs (Table 1).

The sea-level objectives of ODP Leg 166 were

(1) to document the sedimentary record of Neogene and Quaternary sea level changes,
(2) to determine the ages of the major unconformities,
(3) to compare the sedimentary record with the oxygen isotope record of glacio-eustacy (from Site 1006 in the Florida Strait).

The sedimentary facies variations represent the sedimentary response of the carbonate environment to sea-level changes, and together with diagenesis produce petrophysical differences in the sedimentary succession. Thus the petrophysical logs can be interpreted in terms of facies and sea-level. The average core recovery for the leg was 55.3% – sufficient to document the broad facies succession, but the continuous log data are required to pin-point boundaries, make an analysis of the evolution of the cyclicity, and to identify turbidites in low recovery intervals.

In this paper we present a classification of the sediments based on their FMS image facies, calibrated to core, and then present two applications of the FMS using the classification. In the first, a sedimentation rate curve is derived by counting Type 1 – Type 2 alternations and measuring their thickness (cyclo-stratigraphy), and in the second, the potential significance of uranium log peaks is assessed by their location in the FMS-derived facies succession.

The relationship between FMS image and lithology in this setting

The FMS images from Sites 1003 and 1005 were classified into three image facies types (Table 2). The sedimentary processes by which the FMS images are related to lithology and sea-level are illustrated in Fig. 3, and examples of each type are illustrated in Fig. 4 (902–916 mbsf at Site 1003). Details of the sedimentological analysis of the cores are descibed in Betzler *et al*. (in press) and Eberli *et al*. (1997).

From: LOVELL, M. A., WILLIAMSON, G. & HARVEY, P. K. (eds) 1999. Borehole Imaging: applications and case histories. Geological Society, London, Special Publications, **159**, 227–238. 1-86239-043-6/99/$15.00.

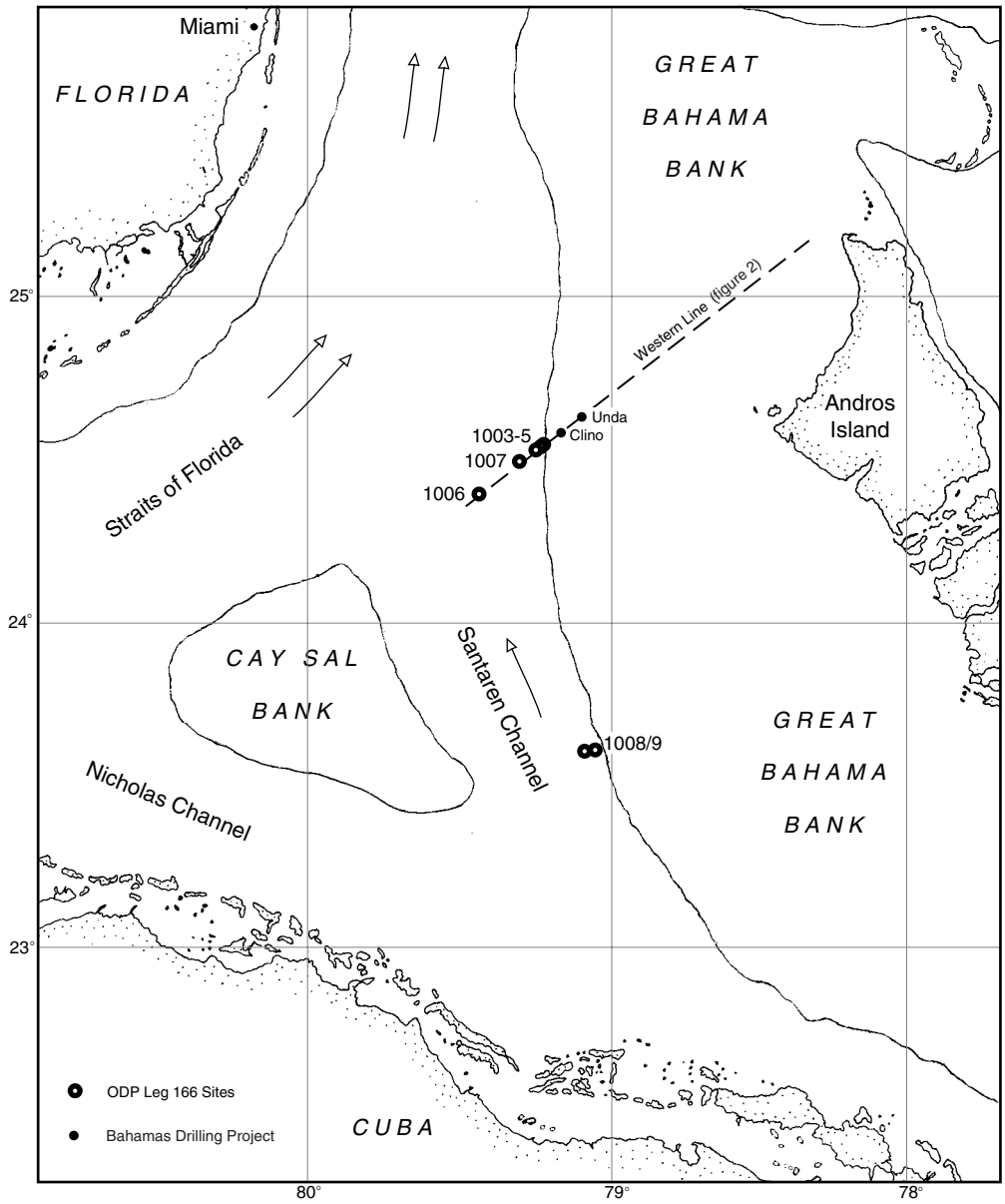

Fig. 1. Location map of the ODP Leg 166 sites (Eberli *et al.* 1997)

Type 1

The Type 1 image facies is conductive (dark on the images), and often has a mottled appearance. It corresponds to dark grey packstones and wackestones, and contains a relatively high proportion of pelagic components. Type 1 sediment contains up to 20% aragonite – it has not been dissolved, remobilized and re-precipitated as cement, hence Type 1 has a high porosity, and burrows which were flattened during sediment compaction. The bioturbation causes the FMS image to be mottled.

Type 2

The Type 2 image facies is resistive (light on the images), and, like Type 1 often has a mottled appearance. It corresponds to well-cemented

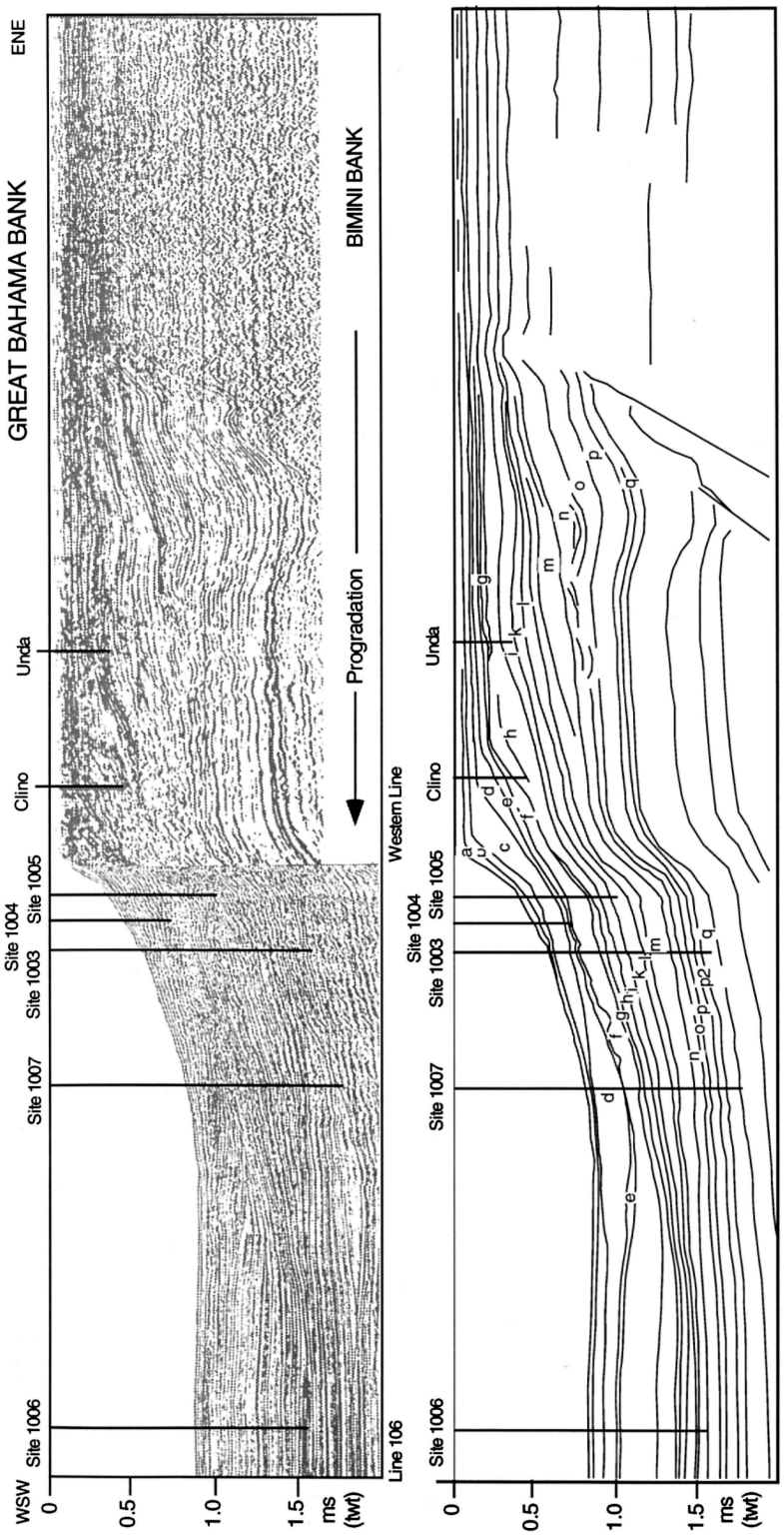

Fig. 2. Seismic section along the Western Geophysical line and its high resolution extension (Fig. 1), with locations of the ODP Leg 166 sites and the Bahamas Drilling Project holes Unda and Clino (drilled in 1990). Below, seismic sequence boundaries and sub-surface geometries. (Eberli *et al.* 1997).

Table 1. *Logging operations during ODP Leg 166*

ODP Hole	1006A	1007C	1003D	1005A, C
Water depth	688 m	648 m	483 m	351 m
Logged interval:				
FMS	103–716	no FMS	107–1050	383–613
conventional	103–718	112–1158	107–1051	89–691

Table 2. *Image, lithological and log character of the three main image facies types.*

	Type 1	Type 2	Type 3
FMS character	conductive, heterogenous (bioturbated)	resistive, heterogeneous (bioturbated)	highly resistive, homogenous or laminated, thin (<1m) beds.
Lithology	dark grey bio-wackestones up to 20% aragonite 5–7% clay flattened burrows	light grey bio-wackestones well cemented 96–99% carbonate burrows retain original shape	calci-turbidites (maybe with current re-working), or occasionally hardgrounds. very well cemented
Log response*			
resistivity	<1 Ω m	1–5 Ωm	>5 Ωm
sonic velocity	2–3 km/s	3–4 km/s	4–6 km/s
density	1.9–2.2 g/cm^3	2.2–2.4 g/cm^3	2.4–2.8 g/cm^3
uranium	4–10 ppm	1–4 ppm	0.5–3 ppm
porosity	40–50 %	20–40 %	25–5 %

* The ranges for the log responses are for the lithified sediment and are a general guide. Most show an overall downhole compaction trend.

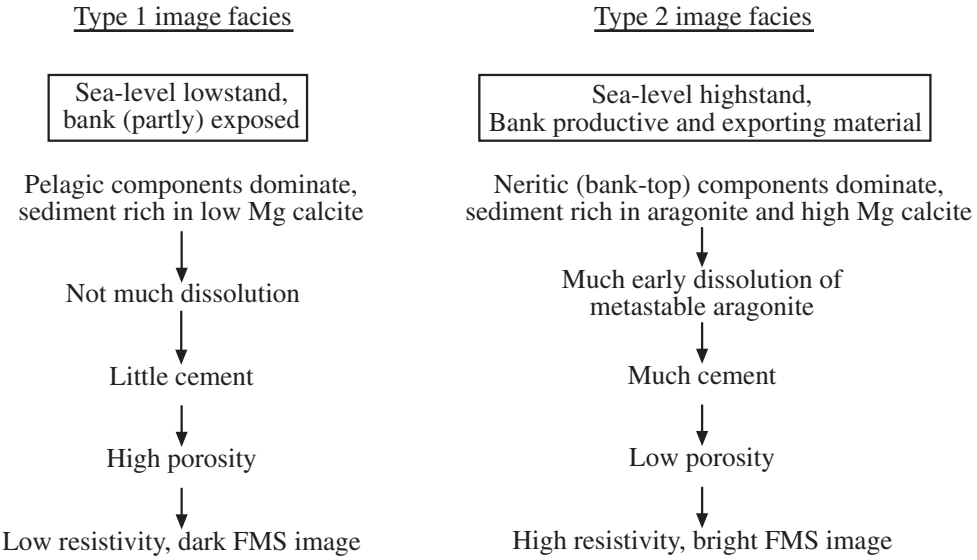

Fig. 3. Schematic diagram showing how the FMS image facies types 1 and 2 are related to lithology and sea-level. Calci-turbidites (Type 3) follow the Type 2 scenario except that they are more cemented and can be deposited during sea-level lowstands as well as highstands.

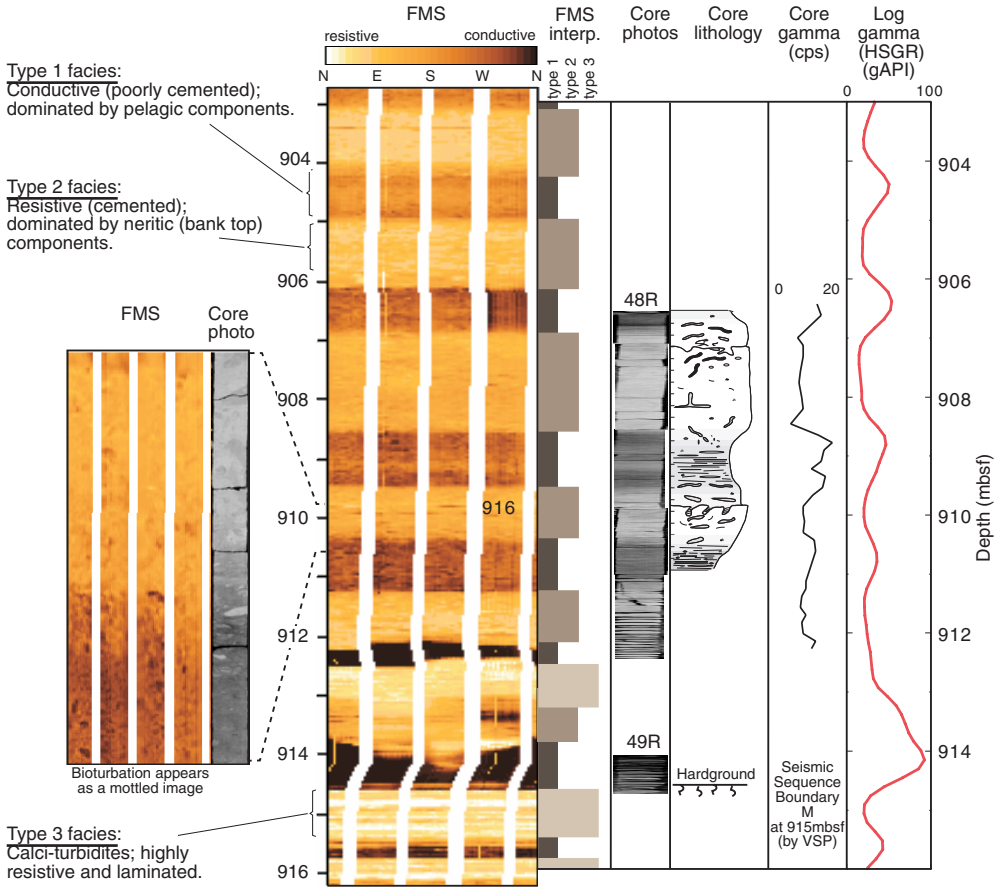

Fig. 4. FMS image from Site 1003, 902–916 mbsf, showing examples of cyclic alternation (902–912 mbsf), calci-turbidites (914.6–916.2 mbsf), a sequence boundary (≈914 mbsf), and bioturbation (detail in the expanded image to the left). The FMS has been divided into Type 1, 2 and 3 sediment in the Interpretation column (see text). Core photographs (compressed), the core lithological log, and the core natural gamma for core 48R are displayed alongside the FMS image. The FMS coverage has been exaggerated (true borehole diameter ≈12 inch).

light grey packstones and wackestones, and is dominated by neritic components from the bank top. Cementation occurred soon enough after deposition to lend the sediment rigidity and thus for the burrows to retain their original shape.

Type 3

The Type 3 image facies is highly resistive (white or very light on the images), either homogenous or laminated, and corresponds to calci-turbidites in the core. Hardgrounds would have a similar FMS response (though they are much rarer), and so are included within Type 3.

Calci-turbidites. The calci-turbidites are usually less than 1 m thick, and generally have well defined tops and bases. Their high resistivity is due to the very high degree of cementation. Less well cemented calci-turbidite layers are distinguished from Type 2 sediment by the lack of mottling (bioturbation) in the Type 3 image.

Hardgrounds. Hardgrounds (and firmgrounds) are recognized in the core as cemented paleosurfaces which have been burrowed down into. They represent periods of non-deposition. In the FMS image, they should appear as a highly resistive layer, however this characteristic alone will not distinguish a hardground from a calci-turbidite, hence in our FMS classification scheme they are both Type 3 (indeed the top surface of a calci-turbidite could also form a hardground). Only two hardgrounds were found in core in the intervals covered by FMS at Sites 1003 and

1005. This is partly due to their preferential non-recovery: the hardness of the hardground relative to the overlying sediment causes a slow-down of the drilling rate, and often associated poor core recovery and a widening of the hole (and hence poor FMS pad contact, for example at 920 mbsf in Fig. 4). Close inspection of the FMS images at depths where hardgrounds were observed in the core showed that hardgrounds and calciturbidites are very difficult to distinguish from each other in the FMS, probably because the FMS image character is partly diagenetic in origin, thus obscuring the detail of the original depositional features.

Early Pliocene sediment

Early Pliocene sediment (120–250 mbsf) has featureless log responses: uniformly low velocity and low resistivity. The hole is too wide in this interval for good FMS pad contact with the borehole walls, but for completeness, we note that this sediment differs from the types described above, in that it is a rapidly deposited, fine-grained, neritic-rich sediment that is uncemented.

Cyclicity in the Middle Miocene

Cyclic alternation was observed in many intervals of the Leg 166 logs and cores. At Site 1003, this cyclicity was particularly well developed in the Middle Miocene seismic sequence m between 738 and 912 mbsf (Fig. 5). The sediment in this interval alternates between Type 1 and Type 2 beds, with occasional interuptions by calciturbidites. We have defined each cycle as comprizing from the base of a Type 1 bed through to the top of the overlying Type 2 bed.

If each cycle represents a constant amount of time, the relative age of the sediment and its sedimentation rate can be determined simply by counting the cycles and measuring their thickness, in the same way that the age of a tree can be found by counting its yearly tree rings. It is well known that the astronomical cyclicities (orbital eccentricity, axial obliquity (tilt), and precession of the equinoxes) control the glacial-interglacial alternations of Plio-Pleistocene climate, and that precessional periodicity is present in Miocene Mediterranean sediments (Hilgen *et al*. 1995, 1997). Given the regularity with depth of the cycles found at the Leg 166 sites, it seems reasonable that each cycle was deposited in a constant duration, at one of the astronomical cyclicities. The astronomical periodicities are known to be reasonably stable at least back to the Miocene (Laskar 1993), but which of those cyclicities is controlling the lithology at Site 1003 is not known *a priori*.

The statically normalized FMS image was used to analyse the bedding. Firstly, the depth to the top and base of the resistive beds were picked, using the 'Borview' module of Schlumberger's Geoframe log interpretation software (dip and azimuth were also determined for each boundary). Between 738 (seismic sequence boundary (SSB) L) and 915 mbsf (SSB M), 122 resistive beds were identified.

Secondly, the resistive beds were classified as either Type 2 or Type 3 sediment, based on the resistivity amplitude, and the internal structure revealed by dynamic normalization of the image. Type 2 were assigned if the bed was mottled (bioturbated sediment), and Type 3 were assigned if the bed was highly resistive and lacked mottling, or if the bed contained laminated surfaces; mostly, Type 3 beds were thinner than the Type 2 beds (Fig. 5). Though the distinction was clear is most cases, there were some beds that could have been classified either way. Sometimes there was insufficient contrast between Type 1 and Type 2 sediment, and sometimes the beds were thin; where this occurred we have chosen to collapse those alternations into 'sub-cycles' of a main cycle. Of the original 122 resistive beds, 19 were Type 3 (calci-turbidites), and 18 were Type 2 but sub-cycles, leaving 85 full cycles; this assignment of the beds is 'version-1'. Sub-cycles and calci-turbidites were not used when calculating ages and sedimentation rates.

Astronomical periodicities were then assigned to the cycles. If each cycle was 41 ka long (the obliquity periodicity), the resulting sedimentation rate would be incompatible with the biostratigraphic dates, being far too slow. Thus the precession of the equinoxes is likely to be the controlling factor, with its characteristic periodicities of 19 and 23 ka. Mean sedimentation rates calculated from these version-1 cycles were 9.1 cm/ka for 23 ka cycles, and 11.0 cm/ka for 19 ka cycles, which are both lower than the sedimentation rate derived from the biostratigraphy (13 cm/ka) (Fig. 6).

A possible cause for the mis-match could be incorrect classification of either Type 3 sediment (calci-turbidite) as Type 2 or a sub-cycle as a full cycle. So in a second attempt (version-2) five of the 85 version-1 cycles were re-classified as calciturbidites, and two as sub-cycles. This version-2 yields what can be regarded as an upper limit to the cyclo-stratigraphic sedimentation rates (9.8 cm/ka for 23 ka cycles, and 11.8 cm/ka for 19 ka cycles). The version-2 rate is still slower than the rate from biostratigraphy (Fig. 6).

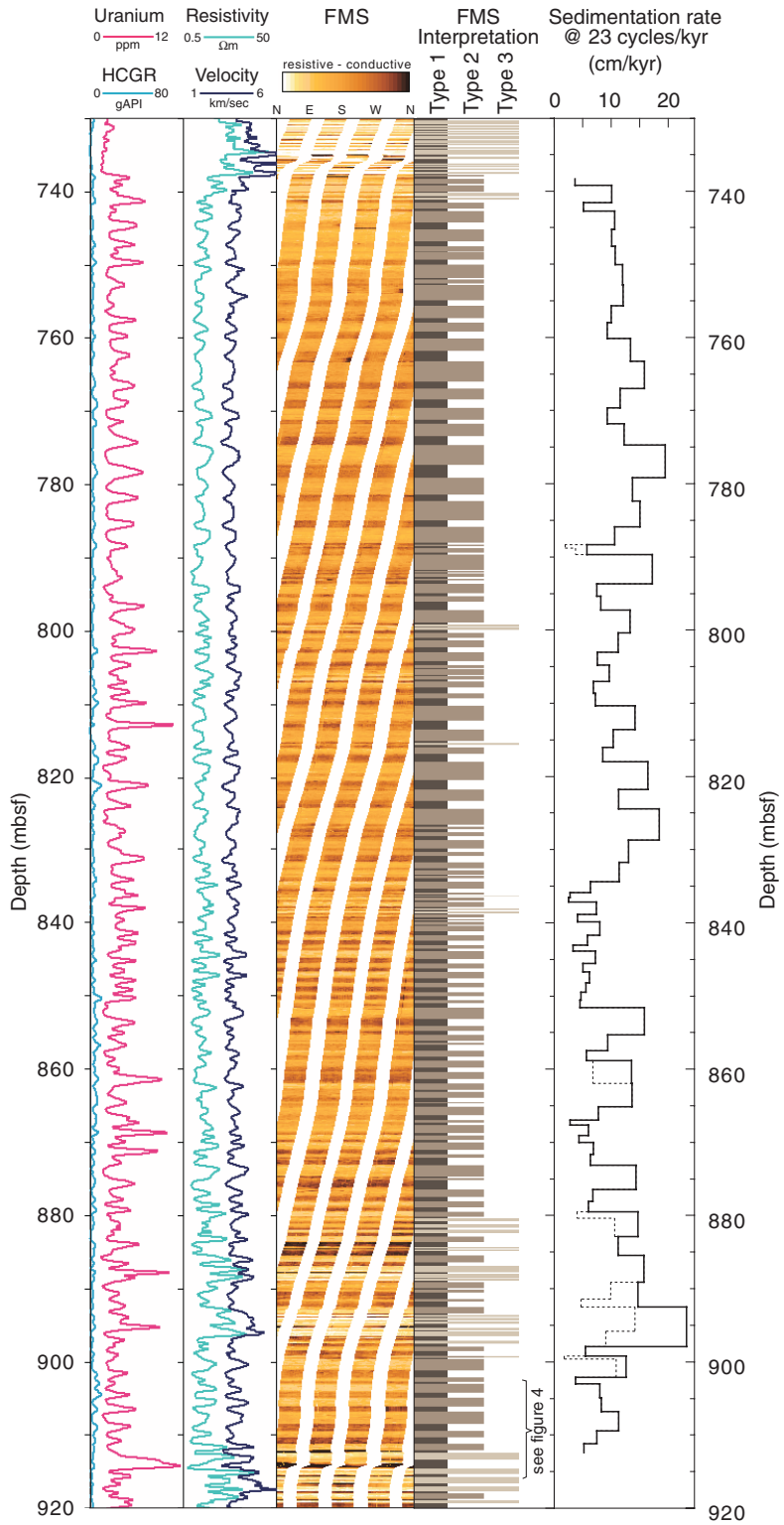

Fig. 5. FMS image of Type 1–Type 2 alternations at Site 1003. Sedimentation rate is derived from the cycle thicknesses in the FMS interpretation (base of Type 1 to base of the next Type 1), and assuming a periodicity of 23 ka/cycle. The solid sedimentation rate curve corresponds to version 2 of the cycles, the version 1 curve is dotted (see text). The FMS coverage has been exaggerated (true borehole diameter ≈12 inches).

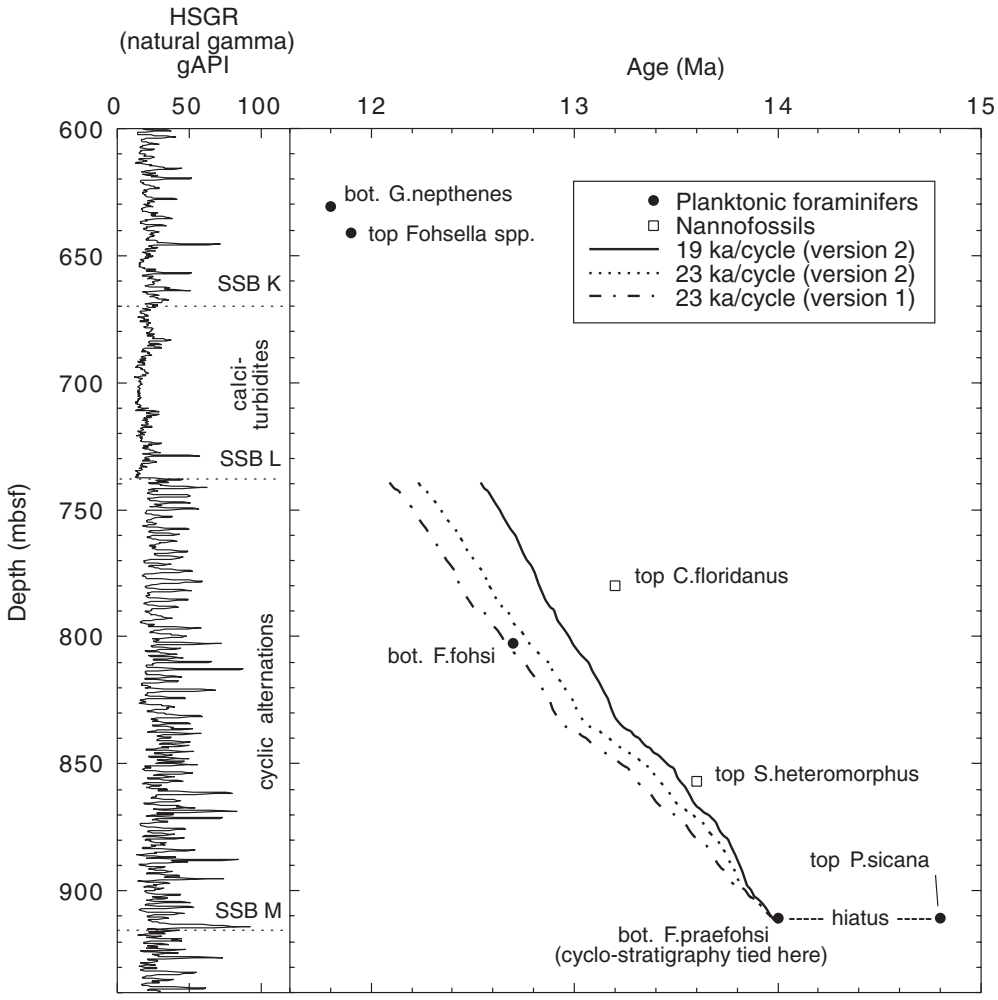

Fig. 6. Age *vs* depth for the Middle Miocene of Site 1003. The sedimentation rates derived from the cyclic alternations are fixed to the end of the hiatus (sequence boundary M). The version 2 curves (19 and 23 ka periodicities) represent the faster end-member of the possible cyclo-stratigraphic sedimentation rates.

We have chosen to fix the floating cyclo-stratigraphy to the end of the hiatus at 912 mbsf, at the first occurrence of the foraminifer *Fohsella praefohsi*, at 14.0 Ma (this is the oldest possible age for the end of the hiatus) (Fig. 6). The 23 ka/cycle cyclo-stratigraphies (version-1 and version-2) are both close to the next foraminifer datum, the first occurrence of *Fohsella fohsi*. However, they are much older than the nannofossil datums (top *Cyclicargolithus floridanus* and top *Sphenolithus heteromorphus*). In the biostratigraphic synthesis (Eberli *et al*. 1997), it is noted that the *C.floridanus* marker (13.2 Ma) occurs at the top of a slumped interval (not apparent in the FMS image), yet it was prefered to the *F.fohsi* foraminifer age (12.7 Ma) when constructing the biostratigraphic age model. The cyclo-stratigraphy indicates that the *F. fohsi* marker is the better, and that both *C. floridanus* and *S. heteromorphus* are unreliable markers at this site.

The slower than expected sedimentation rate between 738 and 912 mbsf requires a higher than average sedimentation rate between 738 mbsf and the next biostratigraphic ages at 630 and 642 mbsf. This is plausible, as this interval is very rich in calci-turbidites, which are likely to have been quickly deposited.

An alternative possibility for the slower than expected cyclo-stratigraphic sedimentation rates

is that the Bergren *et al*. (1995) timescale, on which the biostratigraphy is based, assigns too little time to the middle Miocene: if the middle Miocene were longer, this would enable more cycles to be fitted in. However, this possiblity is beyond the scope of this paper, and the few biostratigraphic ages in this interval and the uncertain accuracy of the cyclo-stratigraphy are not sufficient to make that argument.

A complementary study of the cyclicity at Site 1003 also concludes that the periodicity is precessional (Bernet & Eberli, in press), as do Pirmez & Brewer (1998) for Site 1006.

Uranium peaks and their lithostratigraphic position

Several prominent isolated peaks in the uranium logs from Holes 1003D and 1005C occur coincidently with lithostratigraphic boundaries. The lithostratigraphic position of the uranium peaks, and the possible processes by which uranium becomes concentrated are discussed below to try to explain the occurrence of the peaks and to determine their significance. It has been previously suggested that uranium peaks can mark unconformities, intervals of condensed sedimentation rates, and hardgrounds (Rider 1996).

In the Leg 166 sediments, the natural gamma signal is almost entirely due to uranium, with potassium and thorium (present in clay minerals) contributing only a minor proportion to the total natural gamma log. The CGR log (total natural gamma with the uranium contribution subtracted) is shown in Fig. 5.

The uranium peaks are nearly always located in Type 1 sediment (Figs 4, 5 & 7), and usually occur interbedded between the top calci-turbidites in calci-turbidite-rich units. Quite often a relatively thick layer of Type 1 (pelagic) sediment overlies the calci-turbidite units (Fig. 7 Table 3). The majority of the calci-turbidites are a result of shedding during sea-level highstands, but lowstand calci-turbidites are also significant (Bernet *et al*. 1997) and these cannot be distinguished using the FMS images alone.

Below 740 mbsf at Site 1003, a slightly different regime seems to have been in operation, as the uranium log shows repeated moderately high peaks in the cyclic carbonates. However, a few more prominent peaks that stand out from the background and have the same relationship to the calci-turbidites are still identifiable.

In terms of sequence stratigraphy, uranium peaks can be associated with both sequence boundaries (SSB) (e.g. SSB H, Fig. 7a), and with maximum flooding surfaces (e.g. at 646 mbsf at Site 1003). However, not all the ODP Leg 166 sequence boundaries and flooding surfaces have a corresponding uranium peak.

The few hardgrounds and firmgrounds that were recovered in core at Sites 1003 and 1005 are sometimes accompanied by a uranium peak (e.g. at 914 mbsf at Site 1003 and 640 mbsf at Site 1005), but this is not always the case (e.g. the firmground at 505 mbsf in 1003 has no corresponding uranium peak (Fig. 7b)). The unconformity at 365 mbsf at Site 1003 is marked by a uranium peak, while the corresponding unconformity at Site 1005 is not.

Uranium can concentrate in a variety of ways: in confined, reducing sediments, by reduction of U^{6+} (soluble as the uranyl ion, UO^{2+}) to insoluble U^{4+}; adsorbed onto particles of clay and organic matter; by incorporation into carbonate-fluorapatite, possibly at hardgrounds (Serra 1984). Also, uranium is not included in the lattice of re-precipitated calcite, and is therefore expelled from the more cemented beds.

Colley & Thomson (1985) investigated uranium peaks in recent carbonate-rich distal turbidites on the Madiera abyssal plain. They found that oxidation of the organic carbon in the turbidites mobilizes the uranium (originally adsorbed onto the organic matter) as uranyl carbonate, which is reduced and concentrated into a peak below the oxidation front in the pelagic sediment underlying the turbidite. More than 60% of the uranium originally in the turbidites was re-located in this way. Thus these peaks represent relict oxidation fronts. This appears to be analogous to the occurrence of uranium peaks in Type 1 sediment observed in the Leg 166 logs, except that the gamma peaks occur just below the top of calci-turbidite units, rather than under each individual calci-turbidite. It appears that a change in sedimentary conditions, possibly with a reduced sedimentation rate, is necessary for uranium peak formation. By this process, the uranium peaks might coincide with sequence boundaries (just below the top of the highstand calci-turbidites) or maximum flooding surfaces (just below the top of the lowstand calci-turbidites).

Thus the probable general mechanism for generating the main uranium peaks is re-location of uranium from Type 2 and 3 sediment into the Type 1 layers upon oxidation of organic matter and carbonate diagenesis. Those uranium peaks not associated with the top of calci-turbidite units tend to coincide with other lithostratigraphic changes, or stage boundaries e.g. the mid-late Miocene boundary at 581 mbsf at Site 1005 (Fig. 7c), where the uranium concentration could be in the form of phosphates.

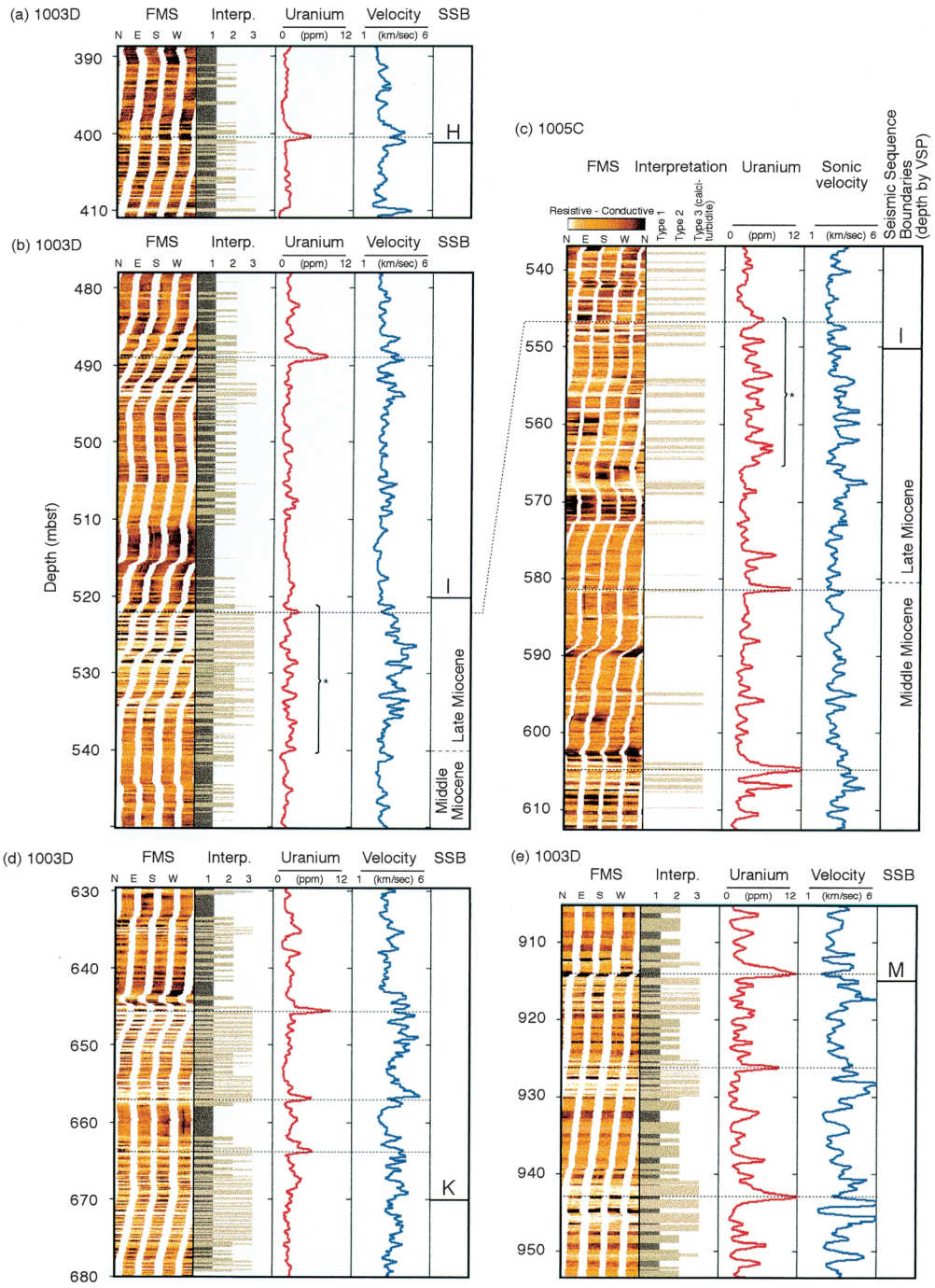

Fig. 7. The position of uranium peaks relative to FMS image facies types and sequence boundaries. In (a) the prominent uranium peak clearly corresponds to SSB H. In (b) (Site 1003) and (c) (Site 1005), there is no single uranium peak corresponding to SSB I but there is a similar uranium pattern (marked *) beneath SSB I; other prominent uranium peaks are marked, one of which is coincident with the Mid–Late Miocene boundary at Site 1005. In (d), SSB K could correspond to the uranium peak and velocity contrast. In (e) there is a contrasting uranium regime to the other examples, but certain peaks still stand out against the background, one of which corresponds to SSB M and a hardground in core. The FMS coverage has been exaggerated (true borehole diameter ≈12 inch).

Table 3. *Position of uranium peaks relative to Type 1 and Type 3 FMS image facies*

Depth to uranium peak (mbsf)	Type 3 sediment below?	Type 1 sediment above?	Lithological setting	Figure no.
Site 1003				
280	no	no	Mudstone to wackestone transition. MFS (maximum flooding surface) ?	
365/370	one	no	Miocene–Pliocene transition. Hiatus ?	
400	yes	yes	Sequence boundary H (402 mbsf).	7a
488	yes	yes	MFS ? Unit boundary.	7b
525–540 (* in Fig. 7)	yes	some	Sequence boundary I (522 mbsf), firmground at 523, Halimeda layer at 532. Interval composed of calci-turbidites.	7b
619	some	yes		
646	yes	yes	MFS, unit boundary.	7d
664	yes	yes	Sequence boundary K (670 mbsf)	7d
729	yes	yes	MFS ?	
915	yes	some	Sequence boundary M (915 mbsf), 2 Ma hiatus, hardground.	4, 7e
943	yes	some	Layer of Halimeda and peloids	7e
974	yes	some	Sub-unit boundary	
984	yes	some		
Site 1005				
491	yes	yes	Sequence boundary H (485 mbsf).	
510	yes	yes		
546–565 (* in Fig. 7)	yes	some	Sequence boundary I (550 mbsf). Interval composed of calci-turbidites.	7c
581	single	yes	Mid-late Miocene boundary	7c
604	yes	yes		7c

One possible cause of the greater frequency of uranium peaks below 740 mbsf at Site 1003 is a higher concentration of organic matter for the uranium to adsorb onto. In Type 1 sediment below 740 m, C_{org} reaches as high as 4%, thought to be mostly enrichment due to hydrocarbon migration (Eberli *et al.* 1997). At these elevated C_{org} contents, complexation with organic matter may also contribute to the uranium peaks.

Conclusions

- FMS images, calibrated to core lithology, can be used to identify pelagic-rich sediment, neritic-rich sediment, and calci-turbidites at the Leg 166 sites.
- Cyclic alternations between pelagic-rich and neritic-rich sediment in the middle Miocene at Site 1003 are controlled by the climatic precessional astronomical period (≈23 ka). Cycle counting yields a cyclo-stratigraphy which suggests that the sedimentation rate derived from biostratigraphy for the interval 740–910 mbsf is too fast.
- Uranium peaks tend to occur just below the top of calci-turbibidite-rich units, and probably represent relict oxidation fronts. They can correspond to sequence boundaries, maximum flooding surfaces, or other lithological boundaries.

We wish to thank Alison Mabillard and Bruce Sellwood for their reviews, Karin Bernet and Christian Betzler for reading early versions of the paper, and Flavio Anslemetti for figs 1 & 2. We also thank Schlumberger engineer Steve Kittredge, and the ODP and SEDCO crews aboard the JOIDES Resolution for their help in obtaining the logs.

References

Anselmetti, F. S., Eberli, G. P. & Zan-Dong Ding (in press). From the Great Bahama Bank Into the Straits of Florida: A Margin Architecture Controlled by Sea Level Fluctuations and Ocean Currents. *Geological Society of America Bulletin*

Bergren, W. A., Kent, D. V., Swisher, C. C. III & Aubry, M. -P. 1995. A revised Cenozoic geochronology and chronostratigraphy. *In*: Bergren, W. A., Kent, D. V., Aubry, M. -P. & Hardenbol, J. (eds.) *Geochronology, Time Scales, and Global Stratigraphic Correlation*. Special Publication Society of Economic Paleotologists and Mineralologists, **54**, 129–212.

BERNET, K., EBERLI, G. P., BETZLER, C. & GILLI, A. 1997. Highstand Versus Lowstand Shedding of Carbonates – new Data for an old Controversy from the Western margin of Great Bahama Bank. *EOS*: *Transactions, American Geophysical Union,* **78**(46), F359.

—— & —— (in press). Spectral analysis on resistivity data along the western Great Bahama Bank (Leg 166, Site 1003). *In*: EBERLI, G. P., SWART, P. K., MALONE, M. J. *et al*. *Proceedings of the Ocean Drilling Program, Scientific Results*, **166**: College Station, TX.

BETZLER C., ANSELMETTI, F., BERNET, K., EBERLI, G., FRANK, T. & REIJMER, J. (in press). Sedimentary variations in space and time along the leeward flank of the Great Bahama Bank (ODP Leg 166). *Sedimentology*.

COLLEY, S. & THOMSON, J. 1985. Recurrent uranium relocations in distal turbidites emplaced in pelagic conditions. *Geochimica et cosmchimica acta*, **49**, 2399–2348.

EBERLI, G. P., SWART, P. K., MALONE, M. J., *et al*. 1997. *Proceedings of the Ocean Drilling Program, Initial Reports*. **166**, College Station, TX.

HILGEN, F. J., KRIJGSMAN, W., LANGEREIS, C. G., LOURENS, L. J, SANTARELLI, A. & ZACHARIASSE, W. J. 1995. Extending the astronomical (polarity) time scale into the Miocene. *Earth and Planetary Science Letters*, **136**, 495.

——, ——, —— & —— 1997. Breakthrough made in dating the geological record. *EOS*, **78**(28), July.

LASKAR, J., LOUTEL, F. & ROBUTEL, P 1993. Stabilization of the Earth's obliquity by the Moon. *Nature*, **361**, 615–617.

PIRMEZ, C. & BREWER, T. S 1998. Borehole electrical images: recent advances in ODP. *JOIDES Journal*, **24**, 14–17.

RIDER, M. 1996. *The Geological Interpretation of Well Logs*. Caithness, Whittles Publishing.

SERRA, O. 1984. *Fundamentals of Well-Log Interpretation (Vol. 1): The Acquisition of Logging Data. Development of Petroleum Science*, **15A**(1) Elsevier, Amsterdam.